JOURNAL OF SPACECRAFT AND ROCKETS
Vol. 46, No. 3, May–June 2009

Demonstration of a Wire Suspension for Wind-Tunnel Virtual Flight Testing

John C. Magill,* Paolo Cataldi,† Joseph R. Morency,‡ and Daniel X. Hammer§
Physical Sciences, Inc., Andover, Massachusetts 01810
and
Riley Burgess¶ and Edward Jeter**
Naval Air Warfare Center, China Lake, California 93555

DOI: 10.2514/1.39188

This paper describes the development of a wire suspension system for dynamic testing of missiles in a wind tunnel. The system restrains the missile, permits motion in 3 rotational degrees of freedom, and measures forces on the model. The apparatus allows testing of missile control systems in the wind tunnel, reducing the cost and risk of a flight-test program. Hydraulic actuators control cable tension and model position. Bearings provide free roll and pitch, whereas yaw motion is created by the cable actuation system and a repetitive-learning controller. The paper describes the cable arrangement, force balance, bearings, closed-loop hydraulic control, and the repetitive-learning controller. Two sets of tests were conducted with the broad ocean area missile (a sidewinder variant) in the High-Velocity Air Stream facility at the China Lake Naval Weapons Center. The tests, conducted at $M = 0.4$–0.6, demonstrate functionality of the system in a series of missile pitch and yaw maneuvers. The learning controller is shown to learn an s maneuver in the yaw plane.

Nomenclature

C_{M_α}, $C_{M_{\dot{q}}}$	=	model stability parameters
I_{yy}	=	movement of inertia of missile about the pitch axis
I_{zz}	=	movement of inertia of missile about the yaw axis
$i_{v,j}$	=	current to jth servo valve
K_d	=	cylinder position loop derivative gain
K_m	=	moment gain in learning algorithm
K_p	=	cylinder position loop proportional gain
ℓ_j	=	position of cable i
ℓ_i	=	starting length for cable i
$N_{i,n}$	=	yawing moment for learning iteration i at time step n
q_j	=	cylinder j measured position
$q_{j,d}$	=	cylinder j desired position
$\tilde{W}_{i,n}$	=	$W_{i,n}$ normalized by its maximum value
$\bar{W}_{i,n}$	=	yawing moment high-pass-filter output in learning algorithm for learning iteration i at time step n
$\dot{x}$, $\dot{y}$, $\dot{z}$	=	model translation rates
ΔT	=	control time step
θ	=	pitch angle
τ_w, τ_v	=	time constant for filters in learning algorithm
$\Psi_{i,n}$	=	yaw motion profile for iteration i at time step n
$\bar{\Psi}_{i,n}$	=	change to yaw motion profile applied to iteration i at time step n

Received 19 June 2008; revision received 7 November 2008; accepted for publication 18 November 2008.

*Principal Research Scientist, 20 New England Business Center. Senior Member AIAA.
†Senior Project Specialist, 20 New England Business Center. Member AIAA.
‡Manufacturing Engineering Manager, 20 New England Business Center.
§Group Leader, Biomedical Imaging, 20 New England Business Center.
¶Missile Integration Specialist, Weapons Division.
**Technical Staff, Weapons Division. Senior Member AIAA.

Introduction

IN AN effort to match test technology to the pace of advancement in maneuverability of missiles, engineers at the U.S. Air Force Arnold Engineering Development Center (AEDC) began many years ago to develop new dynamic wind-tunnel test techniques [1]. These techniques, now known as virtual flight tests (VFTs), are intended to evaluate guidance and control systems, aeroelastic phenomena, and flows around maneuvering bodies. The purpose of the VFT is to provide advanced dynamic test capabilities to developers of missiles and other flight vehicles.

In a VFT, the test article will be supported in the wind tunnel such that it can pivot freely while being restrained from translational motion. The vehicle attitude control system can be tested over a range of flight angles, so that unexpected dynamic behaviors can be identified and control systems can be tested and refined. By permitting preflight control evaluation, VFTs can reduce the risk and, hence, the potential cost associated with flight testing.

In its most basic embodiment, a VFT apparatus must support the test article in the wind tunnel while allowing it to rotate about one or more axes (roll, pitch, and yaw). The rotational damping due to the mount must be small relative to the aerodynamic loads on the vehicle, so that the mount does not render the missile much more stable than the in-flight behavior. In fact, a key use of the device will be to determine whether a vehicle control system is able to maintain stable flight over a range of conditions. Large parasitic damping from the mount would produce false results.

To increase the amount of data available from a test, we have engineered a system that meets the minimum needs and adds a number of sensing capabilities. These include angle measurements and multicomponent aerodynamic load measurements. Because past experience showed that aeroelastic instabilities in the mount structure can be excited during maneuver tests, the new system also includes an active hydraulic damping system.

AEDC and China Lake engineers previously demonstrated an eight-wire system in the High-Velocity Air Stream (HIVAS) facility at China Lake [2]. These tests were performed in the same facility with the same missile as the tests described in this report. Physical Sciences, Inc., (PSI) later demonstrated a small-scale six-wire system in a 40 in. wind tunnel at Georgia Institute of Technology [3]. Drawing on the experience of the previous tests, the latest generation of the wire suspension systems was built and tested. PSI, the Naval Air Warfare Center/China Lake, and AEDC recently completed the

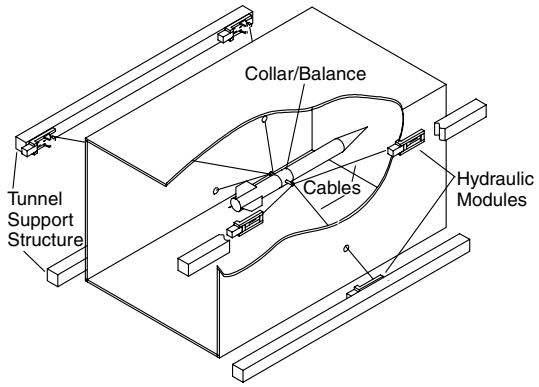

Fig. 1 Configuration of wire suspension system, shown in representative wind-tunnel test section.

most sophisticated virtual flight tests to date. This paper summarizes the system design and then describes several virtual flight tests performed with the broad ocean area (BOA) 1SC PTV-2 air-to-air missile

Figure 1 shows the configuration for the system as it would be applied to a wind-tunnel test section. The system consisted of six cables supporting the model. The model was attached to a collar assembly at the center of the test section. Each cable was attached to a hydraulic cylinder to provide cable pretension and damp elastic oscillations of the cable/model structure and to pull or relax the cable to produce yaw motion.

The collar assembly included pairs of roll and pitch bearings to provide free motion in those axes. The collar also included a strain gauge balance that is able to measure axial, normal, and side forces, as well as yawing moment. The hydraulic actuators imparted yaw to the model by pulling and relaxing the cables. This provided an apparent yaw degree of freedom. A learning controller used yawing moment measurements from the balance, acquired during several repetitions of a maneuver, to determine the yaw motion resulting from a particular set of control inputs. This apparent yaw approach was chosen over the previous approach of incorporating yaw bearings [3] because the structure supporting additional bearings produced substantial aerodynamic interference with the model.

The specific design requirements are summarized here: 1) a maximum normal force of 4000 lb static + 5000 lb dynamic, 2) a maximum axial force of 500 lb static + 400 lb dynamic, 3) a maximum induced motion due to elastic response not to exceed 1 in. and 2 g, 4) a rotational friction torque not more than 10 in. · lb, 5) a 360 deg roll, 6) a ±30 deg yaw, 7) a ±180 deg pitch, and 8) a minimum safety factor of 3.0 based on yield strength.

Sensor and Actuator Suite

The VFT system included sensors to measure desired test data, perform control functions, and maintain safe test conditions. The full sensor suite included 1) a four-component strain gauge balance to sense normal force, axial force, side force, and yawing moment; 2) load cells to sense cable tension; 3) hydraulic actuator position sensors; 4) quadrature encoders to sense roll and pitch angles; and 5) a collar accelerometer to sense model motion.

The VFT collar was designed to accommodate roll and pitch slip rings to carry signals and power across the bearings, but they were not needed for these tests. The balance and accelerometer cables were directly connected because pitch was limited and the model was internally powered.

System Mechanical Design Overview

Figure 2 shows the collar assembly that enabled the model to pitch and roll while measuring axial, normal, and side forces, as well as yawing moment. The test model's fore and aft sections were attached to the model hubs on either end of the collar. They were connected by the roll shaft, which rotates in a pair of bearings. These bearings supported both radial and axial loads. Loads were transmitted to the bearing housing, so that the roll shaft was loaded only by preload tension and roll torsion. Missile bending moments were transmitted between the fore and aft model sections through the balance body. An optical encoder at one end of the bearing housing measures roll angle with a resolution of 0.09 deg.

This collar design provides bearings at a diameter much smaller than the test article, resulting in two key advantages. First, smaller bearings produce less rolling friction. Second, the bearings do not need to match the missile o.d. To change to a model of any diameter larger than the size of the housing, it is necessary only to fabricate a shroud for the bearings that matches the size of the missile (see Fig. 3).

A key component of the bearing selection criteria was the bearing friction torque. Using the manufacturer's data, we estimated the breakaway and dynamic friction under load for each of the aforementioned combinations. Procedures for estimating bearing friction can be found in textbooks [4] and in the manufacturer's literature[††]. Deep-groove ball bearings were chosen for the roll axis. The pitch bearings present a greater challenge in friction, because they must carry the substantial axial load due to cable pretension. Analysis showed that the best choice of pitch bearings is a combination of a ball thrust bearing to carry an axial load and a radial ball bearing to support the radial loads.

To determine whether the anticipated bearing friction is acceptable, we modeled the impact of the static and dynamic friction on a candidate missile model. The model was created using MATLAB®/SIMULINK. The model is a simple rotational spring mass damper. This represents the pitch dynamics of a missile model constrained in a wind tunnel.

The missile used in the simulation had the following properties, estimated by examining published data for a variety of missiles: 1) pitch stiffness (C_{M_α}): −20; 2) pitch damping ($C_{M_{\dot{q}}}$): −500; 3) diameter: 6 in.; 4) length: 60 in.; 5) moment of inertia (I_{yy}): 13 slug · ft^2; 6) freestream velocity: 900 ft/s; and 7) pitch bearing friction: case I: no friction, case II: 12 in. · lb rolling torque and 24 in. · lb starting torque, and case III: 30 in. · lb rolling torque and 60 in. · lb starting torque.

Simulations were carried out for three bearing friction levels (Fig. 4) to predict the response of a model disturbed 10 deg from its trim angle of attack. For case II, which is approximately the bearing friction level estimated for our design, the time history of the pitch angle is nearly indistinguishable from the frictionless case except at very low pitch excursions. This indicates that the bearing friction will not seriously impede the evaluation of the damping parameters. Even in case III, which has nearly twice the friction estimated for our design, the impact on pitch oscillation is modest.

In general, the attachment of a missile to the collar will change the structural properties of the airframe, most notably the bending and torsional stiffness. For the demonstration tests described here, this was not specifically addressed. When aeroelastic characteristics must be accurately recreated in the test, special attention to the roll shaft stiffness and the hub/attachment details will be required. We anticipate that this would include both computer modeling of the elastic properties and tests of the stiffness and natural frequencies of the structure after assembly of the test configuration.

Pitch action was provided by bearings mounted in the cable vertex block. An optical encoder attached to one of these blocks sensed pitch position with a resolution of 0.09 deg. The pitch axle carried approximately 5000 lb of cable pretension load. To avoid overloading the bearing housing and potentially distorting the bearings, a tension box was incorporated in the collar design. This element attached on opposite sides to the pitch axle and provided a mounting point for the balance.

The strain gauge balance [4–8] was formed by a pair of flexure plates that flanked the roll housing. They were instrumented with a total of four full bridges. Fore- and aft-side force bridges sensed both the net side force and yawing moment. A third bridge measured the

[††]Catalog 4000 US, SKF Industries, Inc., Norristown, PA, 1991.

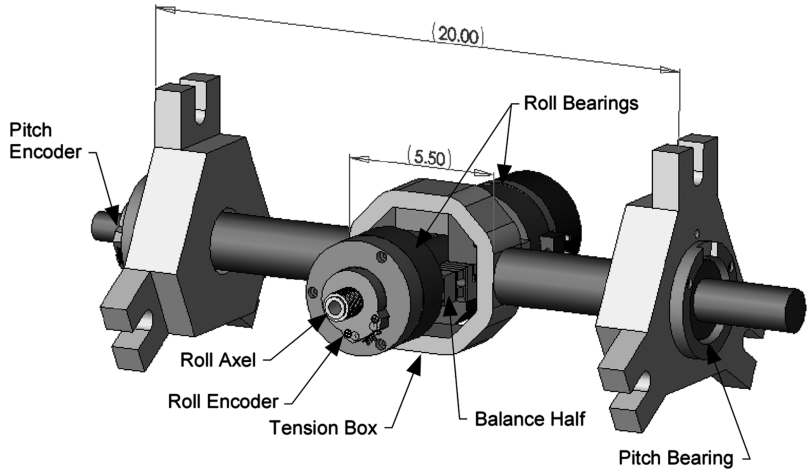

Fig. 2 Collar assembly supporting missile fore and aft sections and providing free pitch and roll. The balance segments were instrumented to provide force and moment measurement.

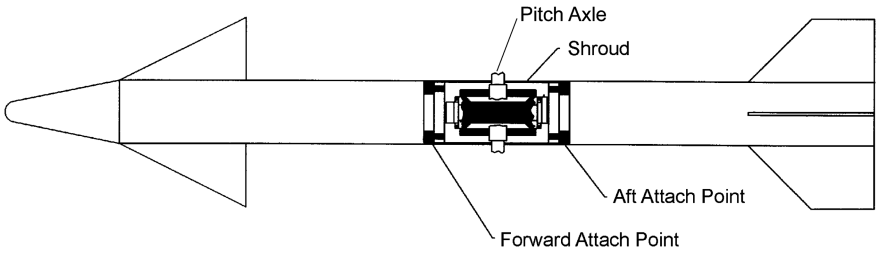

Fig. 3 Missile attachment to collar assembly.

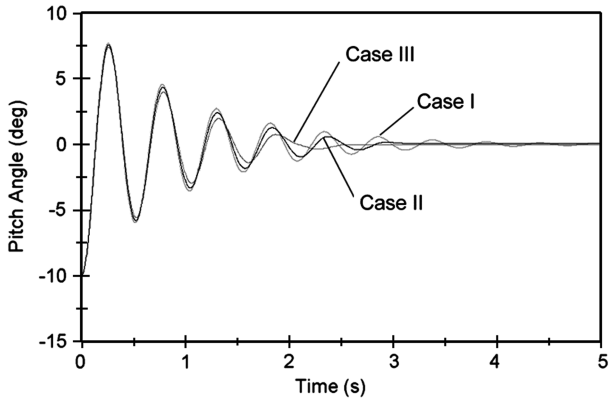

Fig. 4 Simulated pitch response of a model disturbed 10 deg from its trim angle of attack for three different bearing friction levels. Case I: no rolling or starting friction, case II: 12 in. · lb rolling torque and 24 in. · lb starting torque, and case III: 30 in. · lb rolling torque and 60 in. · lb starting torque.

normal force, and the fourth was applied to the main axial force flexure.

To minimize aerodynamic interference, the collar was designed to be as small as possible while supporting the loads at required safety factors. The degree of interference with the flow over the airframe will depend on body diameter, fin geometry, control actuators, and distance of fins and control surfaces from the collar. We did not quantify the effects of the collar on flow over the test vehicle airframe in initial tests, but we recognize this as an important issue that should be addressed in future tests.

The entire balance was made from grade 300 Maraging steel (American Society for Testing and Materials A538) with a yield and ultimate tensile strength of 315,000 and 321,000 psi, respectively. The plates were electron beam welded to the roll housing.

The cables were formed from two sections. A 1/2 in. rigid round steel (17-4 precipitation hardening stainless) rod was attached to the collar and extended past the outer boundary of the test section. Outside of the tunnel, a 1/2 in. flexible steel cable was attached to the solid rod. The cable was a 6×19 extra-improved plow steel wire-core wire rope. The flexible cables were routed over a pulley to provide flexibility in mounting the hydraulic cylinder modules. Forces in the cables were measured using 1210-series load cells from Interface, Inc. The load cells chosen had a rated load range of up to 10,000 lb.

Each cable was pulled into tension by a 2.5-in.-diam hydraulic cylinder with a 3 in. stroke. Flow in and out of the cylinder was controlled by a two-stage servo valve from Moog, Inc.™ Pressure for the system was provided from a 25 HP hydraulic pump. The pump was water cooled and could provide 10 gpm of hydraulic fluid at 3000 psig.

The hydraulic cylinders located at the end of each cable served three purposes. They provided cable pretension control, they imparted yawing motion, and they could be used as part of a control system to damp unsteady oscillations in the structure.

Figure 5 shows how the hydraulic system operated. A hydraulic cylinder was placed in line with each cable. A servo valve controlled flow in and out of the cylinder. The control computer sensed cylinder position and cable tension force and controlled the valve to achieve the force and position objectives.

Unfortunately, a given set of pretensions will not yield a unique positioning of the collar within the tunnel. The positions for pretensioning the cables were determined in the system setup phase. The operator adjusted the cylinder positions using a graphical user interface while monitoring collar position and orientation, as well as the tension.

Multicylinder Control Algorithm

Figure 6 shows the block diagram for the hydraulic control system. At the heart of the algorithm is the position controller, which controls

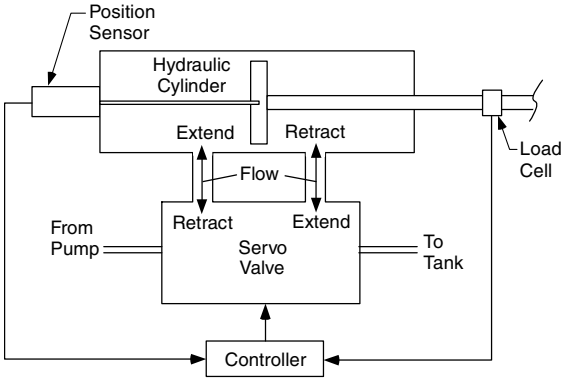

Fig. 5 Components of hydraulic control system.

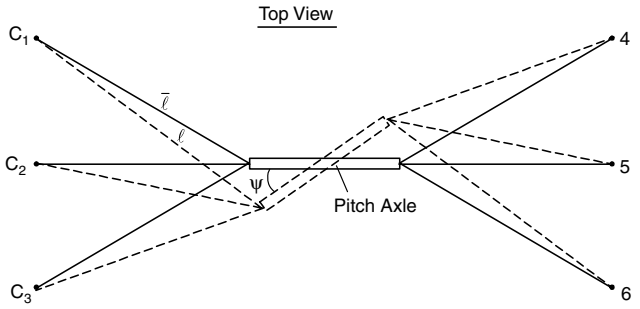

Fig. 7 Top view of cable geometry showing how cable lengths are related to yaw position.

the individual positions of the six cylinders. The controller for each of these six embedded loops had the following form:

$$i_{v,j} = K_p(q_{j,d} - q_j) - K_d\,\dot{q}_j \tag{1}$$

where q_j is the position of the jth cylinder, $q_{j,d}$ is the corresponding desired position, $i_{v,j}$ is the current to the servo valve, and K_p and K_d are control gains.

The desired positions for the six cylinders were determined from three sources, corresponding to the three control functions. The mean position commands were determined from the pretension and setup positions controlled by the user via a graphical user interface. An additional position set representing yaw commands was superimposed on the mean positions. A third set of position commands determined by the damping control system could be added to the others. In the damping controller, a set of gains (K_{dx}, K_{dy}, K_{dz}, and $K_{d\theta}$) determine the damping forces and moment from the measured motion rates. A mapping matrix assigns motions to the six cables to create these damping forces and moments. Although some preliminary demonstration of the damping system was done with the assembled system, it was not used in the wind-on tests and will not be discussed further.

For the yaw control function, position commands were generated by the cylinder motion profiler. As Fig. 7 (a top view of the cable system) shows, the yaw angle ψ can be manipulated by changing the cable lengths ℓ_i. The motion profiler algorithm uses the system geometry to compute the distances from the endpoints of the pitch axle (when yawed to the desired angle) to the cable pulleys. Subtracting these from the distances at zero yaw ($\bar{\ell}_i$) yields the change in cable length and, hence, the required displacement of the cylinder. Cable lengths were not measured explicitly, but once the correct nominal lengths were established in the experimental setup, changes in the lengths could be measured from the hydraulic cylinder position sensors. This requires that we assume that elastic elongation in the cables is constant.

System control functions were implemented using a PC. The PC performs all user interface and fault reporting. Hydraulic control and other real-time activities are performed by a second processor embedded in the PC. The control processor was an 80486 contained on a DAP4200a Data Acquisition Processor from Microstar Laboratories. Communication between the host PC and the DAP takes place over the PCI bus. The DAP 4200a is equipped with 16 single-ended/8 differential analog input channels, which can be sampled at up to 769 kHz total throughput. The board has only two analog output channels and so a pair of four-channel analog output expansion boards was added.

Learning Controller for Yaw

Yaw motion for the wire suspension was created by manipulating cable lengths with hydraulic actuators. The VFT system controller must learn each maneuver to produce the wind-tunnel simulation as follows. The missile autopilot repeats a maneuver several times. The VFT control computer attempts to perform the yaw maneuver commanded by the autopilot. An acceptable initial maneuver, in the absence of better information, is $\Psi = 0$ (no yaw). After each maneuver iteration, the VFT controller updates the yaw motion in response to balance feedback from the previous iteration and performs the revised maneuver. By repeating this process, the learning controller converges on a motion that closely mimics the free-flight behavior of the missile. The "true" maneuver is the one in which there is no yawing moment transmitted to the collar (balance), for this is the situation in which aerodynamic loads are matched by the angular accelerations. This is the yaw maneuver that the missile would undergo in free flight. The algorithm has several advantages, including the prevention of dynamic VFT/autopilot interactions.

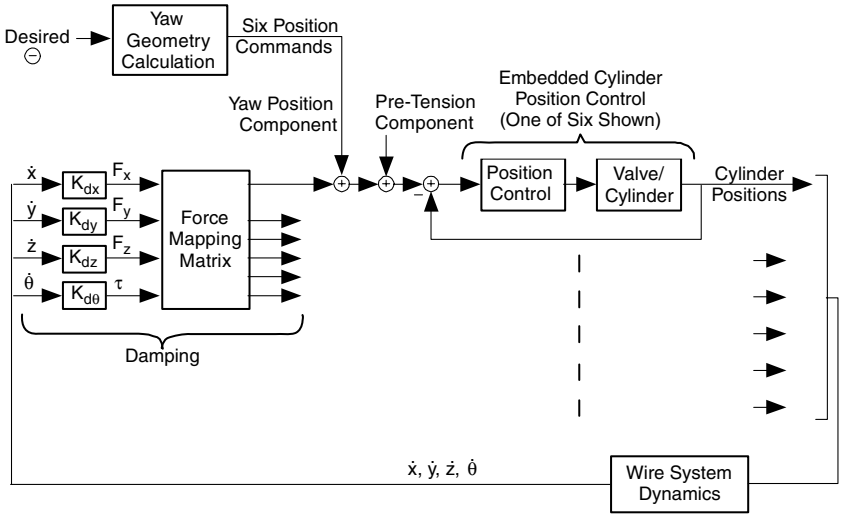

Fig. 6 Block diagram of hydraulic control signal flow.

Figure 8 shows the operation of the learning controller. At each iteration i, the learner uses the results of the previous maneuver to compute a yaw trajectory for the following test. Based on the desired yaw, the cylinder motion profiler calculates a set of cylinder position time histories, and embedded cylinder position loops operate the cylinder position servos during the subsequent test.

We have developed a learning algorithm and tested it in computer simulations [9]. The origins of the algorithm lie in a qualitative understanding of the behavior of the missile, described heuristically here.

We begin with the dynamic torque balance for the missile:

$$I_{zz}\ddot{\Psi} = N \tag{2}$$

where I_{zz} is the yaw inertia, $\ddot{\Psi}$ is the yaw angle (with the double dots indicating its second time derivative), and N is the measured yawing moment. We could simply integrate the measured moment to determine the yaw angle, using the following learning rule:

$$\begin{aligned}
&\ddot{\Psi}_{i+1,n} = N_{i,n}/I_{zz} && \text{(acceleration)}\\
&\dot{\Psi}_{i+1,n+1} = \dot{\Psi}_{i+1,n} + \ddot{\Psi}_{i+1,n}\Delta T && \text{(velocity)}\\
&\bar{\Psi}_{i+1,n+1} = \bar{\Psi}_{i+1,n} + \dot{\Psi}_{i+1,n}\Delta T + \tfrac{1}{2}\ddot{\Psi}_{i+1,n}\Delta T^2 && \text{(yaw change)}\\
&\Psi_{i+1,n+1} = \Psi_{i,n+1} + \bar{\Psi}_{i+1,n+1} && \text{(new yaw profile)}\\
&\text{at } \{n \le 0\}, \quad \bar{\Psi}_{i+1,n} = \dot{\Psi}_{i+1,n} = 0 && \text{(initial condition)}
\end{aligned} \tag{3}$$

Here, the first index denotes the experiment iteration, and the second index denotes the time step (of duration ΔT) within the discrete-time signals. The acceleration is computed from the moment and is integrated to get the yaw rate. The velocity and acceleration are used to compute the change in yaw angle $\bar{\Psi}_{i+1}$, which is added to the yaw angle function from the previous iteration (i) to obtain the yaw angle at the next ($i + 1$) time step. However, the onset of motion would change the moments. The yawing moments that will be applied to the missile result from active control via actuators, as well as the aeroelastic and aerodynamic stability properties. In general, we do not know what these are.

For a missile with positive static stability and damping, the motion would tend to decrease the moment and the imposed velocity would decay. With the algorithm described earlier, the controller would attempt a continuous yaw acceleration because, absent this motion, a constant yaw movement might be observed. Thus, we devised the following yaw change algorithm:

$$\begin{aligned}
&\ddot{\Psi}_{i+1,n} = (N_{i,n}/I_{zz}) \cdot W_{i,n} && \text{(acceleration)}\\
&\dot{\Psi}_{i+1,n+1} = \dot{\Psi}_{i+1,n} e^{-\Delta T/\tau_v} + \ddot{\Psi}_{i+1,n}\Delta T && \text{(velocity)}\\
&\bar{\Psi}_{i+1,n+1} = \bar{\Psi}_{i+1,n} + \dot{\Psi}_{i+1,n}\Delta T + \tfrac{1}{2}\ddot{\Psi}_{i+1,n}\Delta T^2 && \text{(yaw change)}\\
&\text{at } \{n \le 0\}, \quad \bar{\Psi}_{i+1,n} = \dot{\Psi}_{i+1,n} = 0 && \text{(initial condition)}
\end{aligned} \tag{4}$$

Here, $W_{i,n}$ is a weighting function, used to weight response to moment in favor of those that occur just after a change in moment. That is, it is based on the idea that, when a control moment is applied, the missile will move to a new equilibrium condition at which the moment is minimized until the applied moment changes. The weighting function is computed by first processing the first backward difference of the moment with a low-order filter:

$$\begin{aligned}
&\bar{W}_{i,n} = (N_{i,n} - N_{i,n-1})(1 - e^{-\frac{\Delta T}{\tau_w}}) + \bar{W}_{i,n} e^{-\frac{\Delta T}{\tau_w}}\\
&\bar{W}_{i,n} = 0 \quad \text{for } \{n = 0, \ -1\}
\end{aligned} \tag{5}$$

and then normalizing it by its largest value:

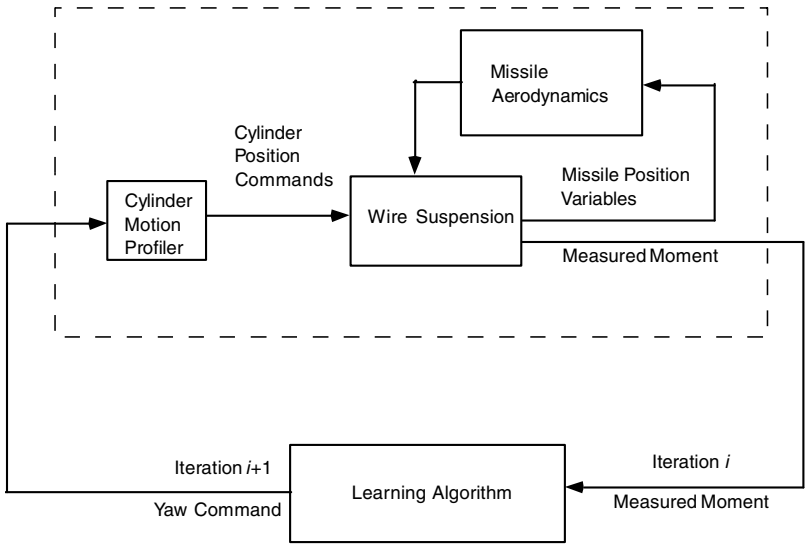

Fig. 8 Learning-controller signal flow.

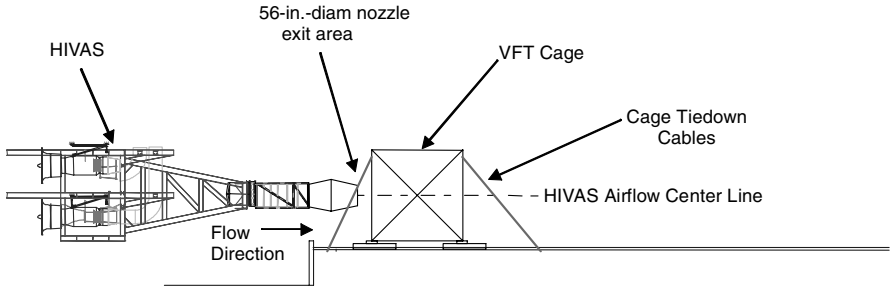

Fig. 9 HIVAS Facility at Naval Air Warfare Center, China Lake, California.

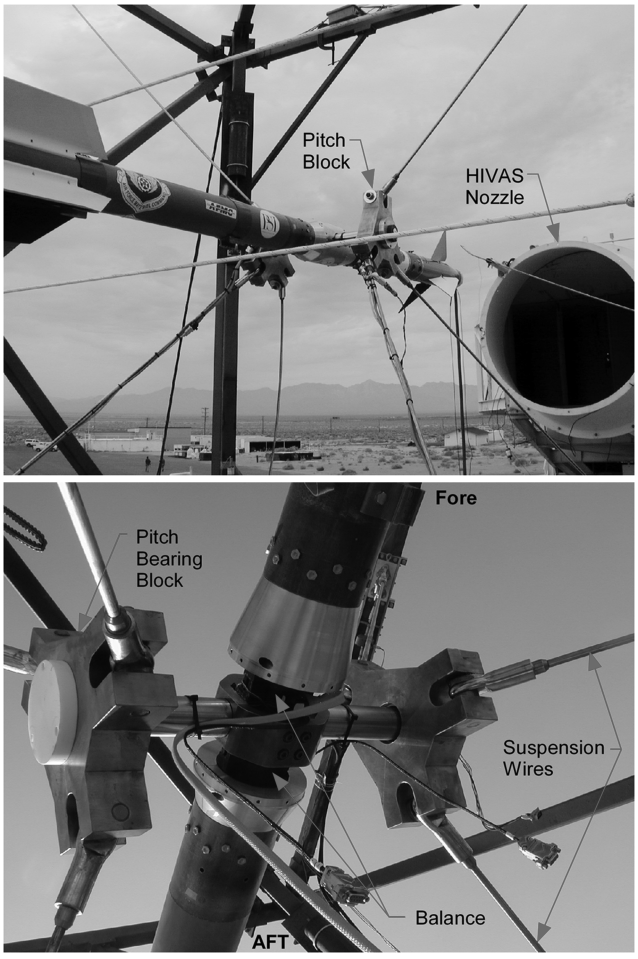

Fig. 10 BOA missile model attached to VFT collar.

$$W_{i,n} = |\bar{W}_{i,n}| / \max(\bar{W}_{i,n}) \tag{6}$$

The filter is a low pass in series with a differentiator, so that it passes changes in the moment but decays to zero output if the moment is constant. The decay time is characterized by the time constant τ_W.

This learning law also incorporates an exponential velocity decay term, characterized by the time constant τ_v. The combination of the weighting filter and the velocity filter is such that, under constant moment, the acceleration and velocity both decay to zero.

Note that the stated assumptions about missile stability are not always true, and we must add a term to accommodate this inaccuracy. The final step in the learning law in Eq. (4) is

$$\Psi_{i+1,n} = \Psi_{i,n} + \bar{\Psi}_{i+1,n} - K_m N_{i,n} \tag{7}$$

where the new term is proportional to the measured moment by the constant K_m.

Test Facility

The tests were conducted in the HIVAS facility at the Naval Air Warfare Center, China Lake, California. HIVAS is part of the Weapons Survivability Laboratory. The facility, shown in Fig. 9, produces a free jet with air ducted from the bypass fans of four TF33 P11 turbofan engines. As configured for this test, HIVAS can produce a 56-in.-diam jet at speeds up to 550 kt. HIVAS can be rotated to face a number of test pads. Air exhausts into the desert environment. The wire suspension system was attached to a steel frame that represented the structure around a wind-tunnel test section.

Broad Ocean Area Missile Model

The BOA-1SC PTV-2 model was chosen because it had been used in previous wire suspension tests at HIVAS and because parts were available for use in the test. It is an advanced variant of the AIM-9 Sidewinder. Figure 10 shows the model geometry. For these tests, the hot-gas servomotors in the missile were powered from a compressed-air bottle located at the aft end of the missile in the rocket motor casing. The weight of the bottle accounted for the missing propellant, allowing the c.g. to be located at a midburn position, coinciding with the location of the pitch axle. A slip ring at the back of the model provided signal and power transmission.

The missile autopilot was equipped with rate feedback, and absolute angle measures were not available. The effect of this on the test results will be seen later. When, for example, the missile is programmed for steady level flight, the controller was attempting to

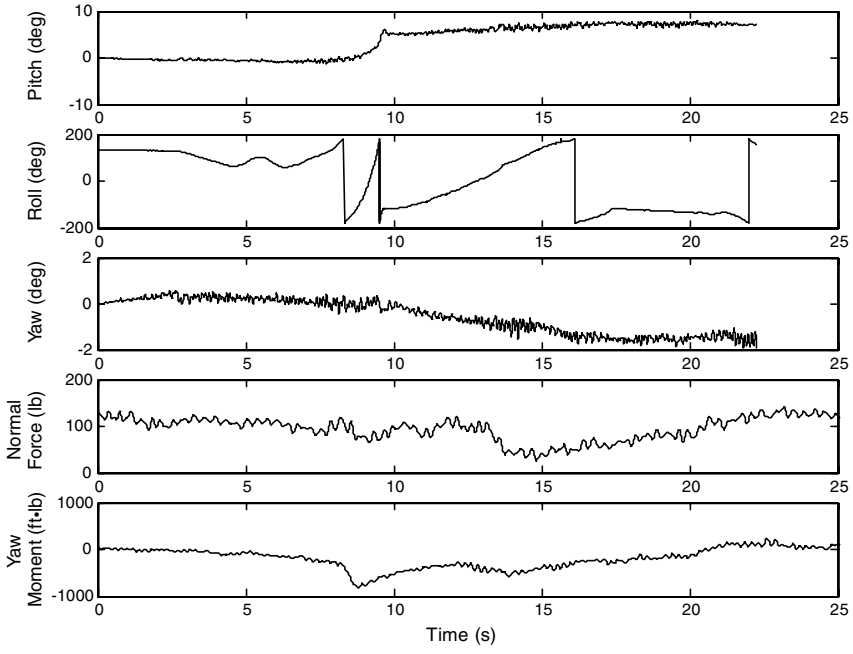

Fig. 11 Motion and force measurements on the model during test 2: 350 kt flow velocity with autopilot programmed for zero-pitch rate.

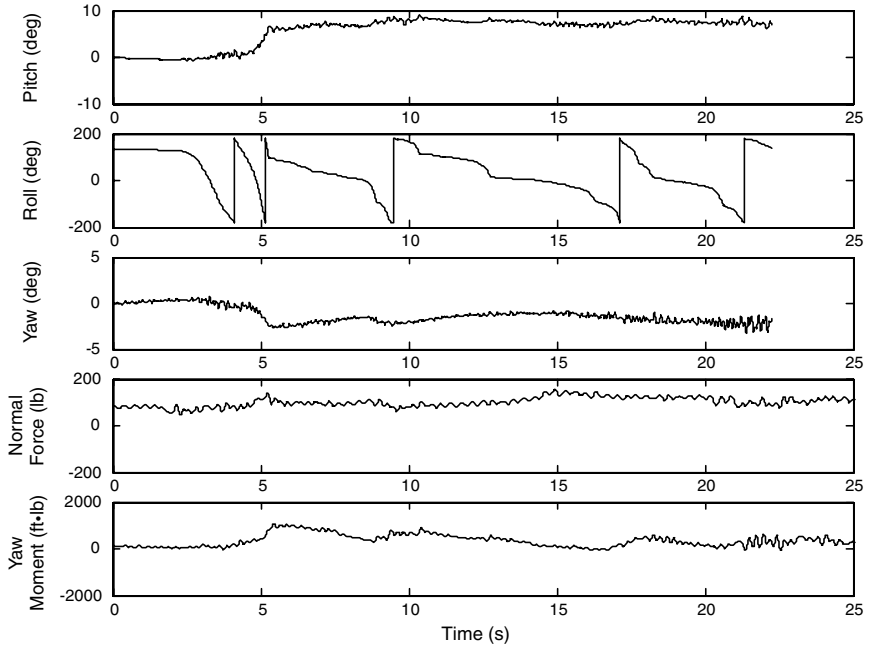

Fig. 12 Motion and force measurements on the model during test 3: 400 kt flow velocity with autopilot programmed for zero-pitch rate.

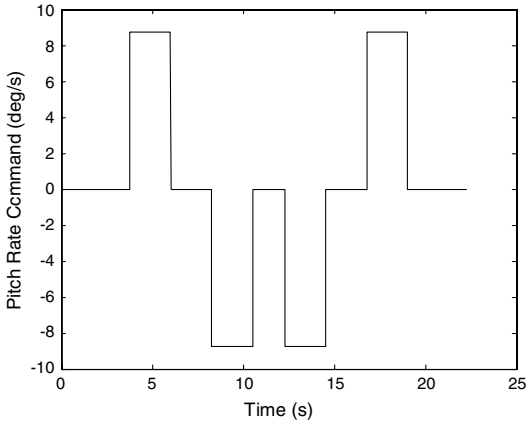

Fig. 13 Pitch motion command for test 6 (see Fig. 14).

hold a zero-pitch rate. When the missile is disturbed from a pitch angle of $\Psi = 0$, the controller will stop the pitch motion (restore $\dot{\Psi}$ to zero) but will not return the missile to $\Psi = 0$. In fact, the autopilot will fight a return to a level orientation because this would involve a nonzero-pitch rate. The control in the pitch and yaw planes are identical, except when a maneuver is commanded in one of them.

One hope for these tests was to reproduce the roll locking observed in-flight tests. Roll lock is a behavior wherein the missile, which rolls freely at low angles of attack, stops rolling suddenly when the angle of attack increases. Demonstration of roll lock was important because it would show that key missile stability characteristics could be recreated in a VFT.

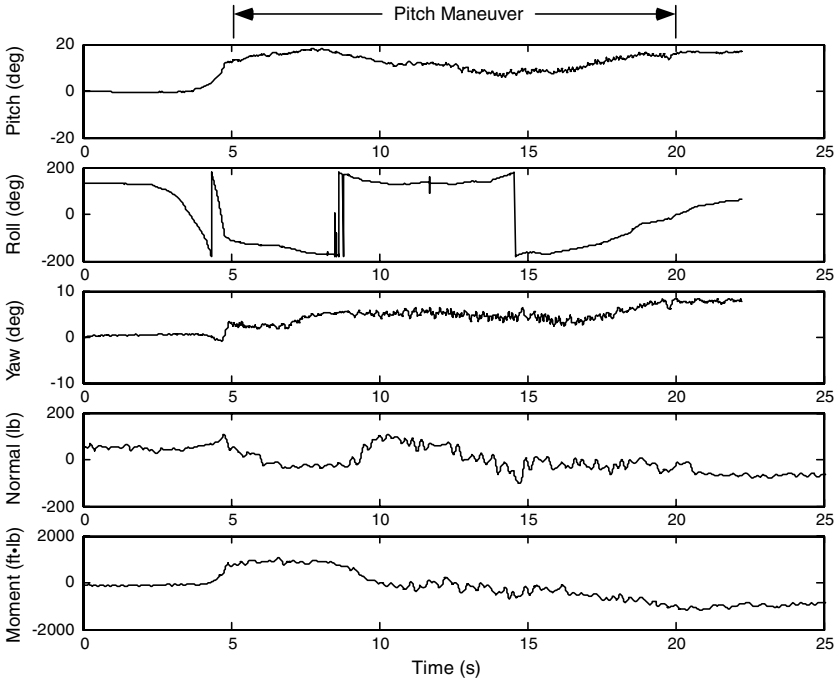

Fig. 14 Motion and force measurements on the model during test 6: 350 kt flow velocity with an s-turn maneuver in the pitch plane.

Wind-On Tests

Data Acquisition

Data were acquired by two methods during the tests. All signals available to the VFT computer were recorded at 416 Hz (at 2400 μs intervals). Other signals were recorded by the missile telemetry system. These signals were logged at 1390 Hz (at 720 μs intervals).

Test Procedure

Each test began with the missile in a zero-pitch condition. A ring on the end of a rod was placed over the missile nose. A person standing ahead of the test frame and below the air stream held the rod.

The facility operator brought the airflow velocity to the desired condition. The missile operator powered up the missile, activated the air supply, switched the missile to operation from internal power, and then disconnected external power. The autopilot was initiated by removing the external power. The missile operator would then give the command to remove the nose ring. The ring was pulled away from the missile, and the test flight began.

The test team completed seven virtual flights during the first test window at HIVAS. The tests are summarized next. Figures 11–17 contain several of the recorded variables for the tests.

The intent of the test sequence was to demonstrate proof of concept. Although the balance was calibrated in a single-axis load

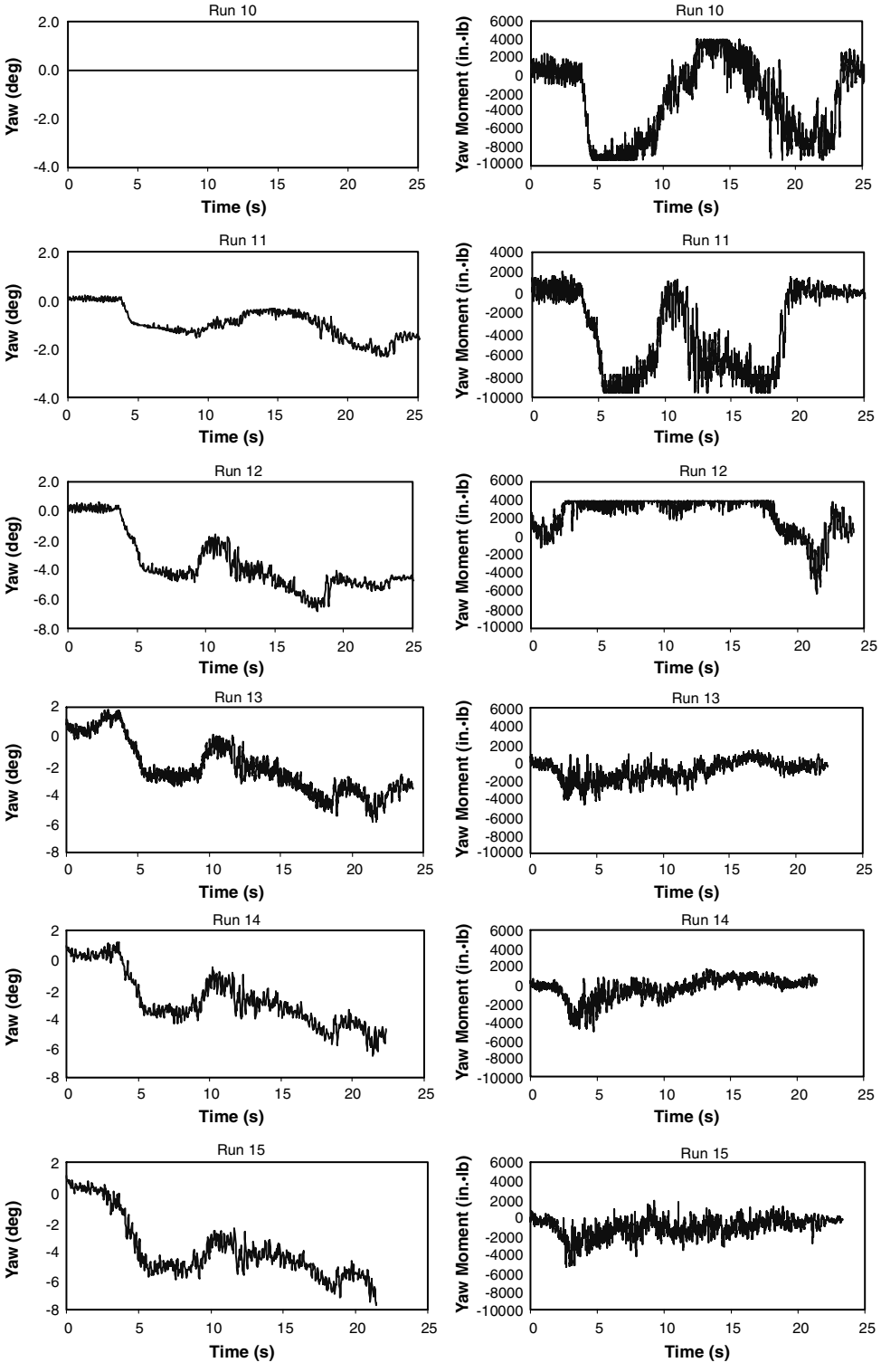

Fig. 15 Comparison of commanded yaw and measured moment for six learning iterations.

apparatus, we did not apply test loads on the installed balance or otherwise attempt to assess the load measurement accuracy. Thus, we make no statements about load measurement accuracy. The qualitative trends in the data do demonstrate the system function.

Results and Discussion

Test Case Summaries

Test 2 (Fig. 11):

Flight control program: pitch rate = 0

Velocity: 350 kt

The missile held a 0 angle of attack for about 8 s. It rolled rapidly for about 1.5 s. There was then a pitch up to about 5 deg. The missile roll locked in this position and approximately held its attitude until the autopilot program ended. Roll locking consists of zero or near zero roll rates. We observed mild cable vibration and some body bending, but all systems functioned properly.

Balance and inertial sensors onboard the model show an oscillation in yaw at about 9 Hz. This probably involves missile aeroelastic characteristics coupled with the elasticity of the mount.

Test 3 (Fig. 12):

Program: pitch rate = 0

Velocity: 400 kt

The behavior was similar to that of test 2. The autopilot was able to hold the pitch rate at zero for long periods. After a pitch up to about 5 deg, the missile again roll locked. There is still some occasional rolling, wherein the BOA would roll about 30 deg suddenly and then stop or roll very slowly. This test demonstrated that we could test at 400 kt.

Test 6 (Figs. 13 and 14):

Program: pitch cycle (s turn)

Velocity: 350 kt

The pitch rate command for this flight can be seen in Fig. 13. The missile can be seen to execute the maneuver in Fig. 14. Although we do not have flight data against which to quantitatively benchmark the result, it shows that the constrained model can execute a programmed maneuver.

All three of these tests show both yaw excursions and yawing moments, although the yaw motion feature was not activated. The excursions are a result of compliance in the cable systems. The yawing moment results as the autopilot attempts to prevent additional yaw motion (i.e., nonzero-yaw rate).

Learning Controller Tests

Experiments to demonstrate the operation of the learning controller and the upgraded balance took place in the HIVAS facility using the BOA missile described earlier, but approximately 9 months after the initial tests. Between the test sequences, the balance was modified for greater sensitivity in the lateral plane. The experimental series consisted of eight virtual flights.

Tests 10–15, again conducted at 350 kt, were the runs in which iterative learning was attempted. The missile controller was commanded to perform the horizontal-plane s maneuver. In run 10, the yaw was held at 0 deg. It was updated in subsequent runs based on the measured yaw restraining moment until the yaw moment was small.

Table 1 Learning law parameters

Run	I (slug · ft^2)	τ_v, s	τ_w, s	K (deg·m/N)
10	500	0.01	0.005	−0.0002
11	500	0.01	0.005	−0.0003
12	500	0.01	0.005	−0.0003
13	500	0.01	0.005	−0.0003
14	500	0.01	0.01	−0.0003

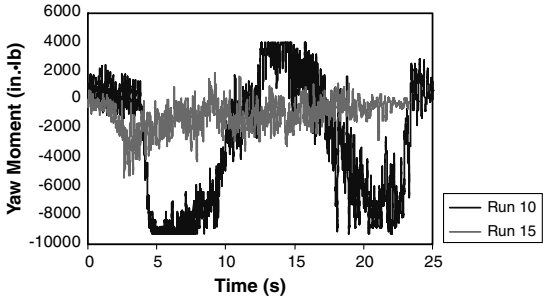

Fig. 16 Comparison of measured moment for the first (run 10) and last (run 15) learning iterations.

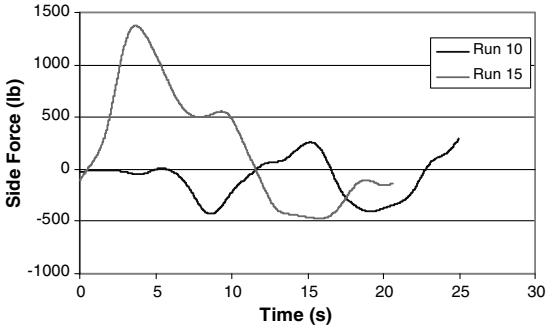

Fig. 17 Comparison of (filtered) side force in runs 10 and 15.

Time permitted only a single training sequence, but the initial sequence was sufficient to demonstrate the function of the learning algorithm.

Figure 15 shows the results of the learning iterations. The learning law parameters are shown in Table 1. For each run, the plots show the measured moment and the yaw attempted by the VFT controller for each case. In run 10, the moment is slightly saturated. It was nevertheless useful for updating the yaw command.

In the first attempt at learning, the algorithm overcorrected the yaw, resulting in the badly saturated moment measured in run 11. This is corrected in the subsequent run by reducing the balance gains and increasing the calibration parameters. Run 13 shows only minor changes in the yaw.

Figure 16 compares the moment measured in runs 10 and 15. The controller has substantially reduced the measured moment by identifying the appropriate yaw time history. This plot is the showpiece from this test sequence in that it captures the ability of the algorithm to iteratively reduce the measured yaw.

Figure 17 compares the side force measured in runs 10 and 15. The side force measurements have been filtered in postprocessing. This demonstrates the ability of the improved balance to measure side forces. In run 10, the side force was small. In run 15, it is much larger because the missile is executing the s maneuver in the yaw plane.

We conclude from the reduction in yawing moment with each increasing iteration that the controller is learning the maneuver. We lack a solid benchmark in the pitch plane with which to compare the result, but the similarity in trends corroborates the yawing moment data. The only significant deficiency of the demonstration is that the algorithm was unable to correct the initial peak in the yaw moment within the number of iterations available.

Conclusions

The test technique described here provides a means of testing missile guidance and control systems in the wind tunnel. Test experience has shown safe operation of the system using an air-to-air missile, demonstrating that dynamic characteristics such as roll locking, which appeared in flight tests, can be recreated in the wind tunnel. The tests showcased a new balance with pitch and roll freedom. Hydraulic control provides yaw and cable tension control, with the option to damp structural oscillations using accelerometer

feedback. The latter has not yet been demonstrated. The sequence of virtual test flights demonstrated a repetitive-learning controller that uses balance feedback to simulate yaw maneuvers. Much of the system, including the hydraulic modules, cable assemblies, and pitch-roll collar, could be put into service in wind-tunnel tests. The measurement techniques and the learning controller have been demonstrated at a basic level, but more test experience is required to refine these methods.

Future work should include testing with a model that can sustain longer runs, refinement of dumping control for the cables, and tests in which forces or flows are compared with those for sting-mounted models to quantify aerodynamic interference.

Acknowledgments

This material is based on work supported by the U.S. Air Force Arnold Engineering Development Center (AEDC) under contract no. F40600-01-C-0015. The contract monitor is Ronald Bishel. The authors thank Frank Steinle, Clark Lawrence, and Ben Mills of Sverdrup Technology, Inc./AEDC for their helpful input. Any opinions, findings, and conclusions or recommendations expressed in this material are those of the authors and do not necessarily reflect the views of the U.S. Air Force Arnold Engineering Development Center.

References

[1] Ratliff, C. L., and Marquart, E. J., "An Assessment of a Potential Flight Test Technique: Virtual Flight Testing," AIAA Paper 95-3472, Aug. 1995.

[2] Lawrence, C., and Mills, B., "Status Update of the AEDC Virtual Flight Testing Development Program," AIAA Paper 2002-0168, Jan. 2002.

[3] Magill, J. C., and Wehe, S. D., "Initial Test of a Wire Suspension Mount for Missile Virtual Flight Testing," AIAA Paper 2002-0169, Jan. 2002.

[4] Brandlein, J., Eschmann, P., Hasbargen, L., and Weigand, K., *Ball, and Roller Bearings: Theory, Design, and Application*, Wiley, Chichester, England, UK, 1999.

[5] Graewe, E., and Ewald, B. E., "Design and Construction of Internal Balances for the German/Netherlands Wind Tunnel (DNW)," *First International Symposium on Internal Strain Gauge Balances*, NASA Langley Research Center, Hampton, VA, March 1999, pp. 525–541.

[6] Rhew, R. D., "NASA LaRC Strain Gage Balance Design Concepts," *First International Symposium on Internal Strain Gauge Balances*, NASA Langley Research Center, Hampton, VA, March 1999, pp. 41–52.

[7] Mole, P. J., "Development of a Six-Component Flexured Two-Shell Internal Strain Gage Balance," AIAA Paper 93-0793, Jan. 1993.

[8] Crandall, S. H., Dahl, N. C., and Lardner, T. J., *An Introduction to the Mechanics of Solids*, 2nd ed., McGraw–Hill, New York, 1978.

[9] Magill, J. C., Cataldi, P., Morency, J. R., Hammer, D. X., Burgess, R., and Jeter, E., "Active Yaw Control with a Wire Suspension System for Dynamic Wind Tunnel Testing," AIAA Paper No. 2005-1295, Nov. 2004.

M. Miller
Associate Editor